

pubs.acs.org/acsaelm Article

# High-Acoustic Sensitivity Radiopure Piezoelectric Materials for Dark Matter Detection

Min Gyu Kang, Yongke Yan, Deepam Maurya,\* Hyun-Cheol Song, Lijuan Yang, Ilan Levine, Edward Behnke, Haley Borsodi, Drew Fustin, Aman Nanda, Juan I. Collar, and Shashank Priya



Cite This: ACS Appl. Electron. Mater. 2023, 5, 6595–6602



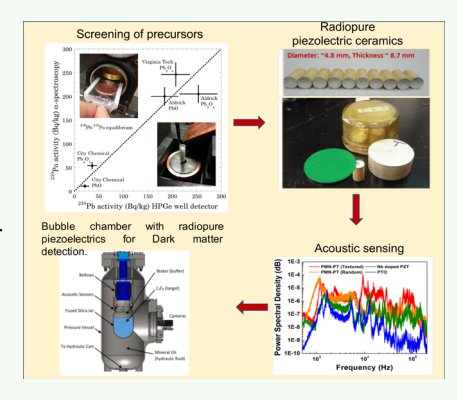
**ACCESS** 

III Metrics & More

Article Recommendations

s Supporting Information

ABSTRACT: Piezoelectric materials are used to fabricate acoustic transducers for bubble chambers in search for particles of dark matter. It has been shown that bubbles initiated by nuclear recoils emit acoustic radiation distinguishable from the phase transitions caused by alpha-decay—the main background noise in such searches. However, these piezoelectric materials must exhibit ultralow radioactivity to minimize the neutron background for dark matter detection while possessing high acoustic sensitivity. Here, for the first time, we demonstrate radiopure high-performance piezoelectric ceramics meeting the criteria for acoustic sensing. The screening of radiopure precursors is performed to identify those with low <sup>238</sup>U, <sup>232</sup>Th, and <sup>210</sup>Pb contents. Using the radiopure precursors, piezoelectric ceramics with varying compositions are synthesized, and their electromechanical acoustic sensing performance is evaluated. Multiple synthesis modifications such as doping and texturing are utilized to tailor the piezoelectric coefficients of the piezoelectric ceramics, and the relationship



between the piezoelectric coefficients and acoustic sensing performance of the ceramics is investigated. Acoustic transducers fabricated using textured  $Pb(Mg_{1/3}Nb_{2/3})O_3-PbTiO_3$  (PMN-PT) ceramics are found to exhibit superior acoustic sensitivity due to their high piezoelectric transduction coefficient ( $d_{33} \times g_{33}$ ). This study demonstrates a useful figure of merit (FOM) for acoustic sensing in bubble chambers.

KEYWORDS: piezoelectric ceramics, texturing, acoustic sensing, radiopure, dark matter, bubble chamber

### INTRODUCTION

Piezoelectric materials have been widely used in sensors, actuators, transducers, and energy-harvesting devices. 1,2 Owing to their inherently high acoustic sensitivity, we have been exploiting them for capturing the acoustic emissions in bubble chambers for dark matter detection.<sup>3,4</sup> In bubble chambers (Figure 1),5,6 a target liquid is heated above its boiling temperature, driving it into a metastable state. When an incoming particle causes a nucleus in the liquid to recoil, the dense energy deposition along the track of the ionized nucleus causes an explosive phase transition to a gas, which amplifies tiny energy (of the order 1 keV) into a detectable acoustic signal. Recently, it was discovered that the acoustic emissions from bubbles initiated by high-energy neutron scattering in the liquid (which mimics dark matter scattering with nuclei) are distinguishable from events initiated by alpha-decay of radioactive nuclei (radioactive decays cause louder bubbles), which allows event-by-event discrimination of the main background to dark matter detection. To sense the acoustic emissions from the bubbles in larger chambers, piezoelectric transducers with enhanced sensitivity are desirable.3 The piezoelectric elements should be radiopure (to reduce their contribution to background radiation) with a superior and stable piezoelectric response over a wide temperature range

(-20-100 °C) and frequency range (1-300 kHz). Commercially available piezoelectric materials have been found to have alpha-emitters from the  $^{238}$ U ( $3.95\pm0.43$  ppm) and  $^{232}$ Th ( $1.18\pm0.15$  ppm) chains, which are sufficient to generate a significant neutron background via the ( $\alpha$ , n) reaction. To solve this issue, starting materials (used for the synthesis of the piezoelectric materials) need to be screened for lower  $^{238}$ U and  $^{232}$ Th contents.

Controlling the background becomes increasingly challenging with the increased numbers of chemical elements in the perovskite-based piezoelectric material. This creates a fundamental issue since piezoelectric coefficients are dependent upon the number of elements, as shown in Figure 2a.  $^{9-12}$  The Curie temperature ( $T_{\rm c}$ ) shows the opposite trend (more prominent for lead-based materials), decreasing with an increasing number of elements in the composition, as shown in Figure 2b. There is a balance between the number of

Received: August 14, 2023 Revised: November 28, 2023 Accepted: November 28, 2023 Published: December 12, 2023





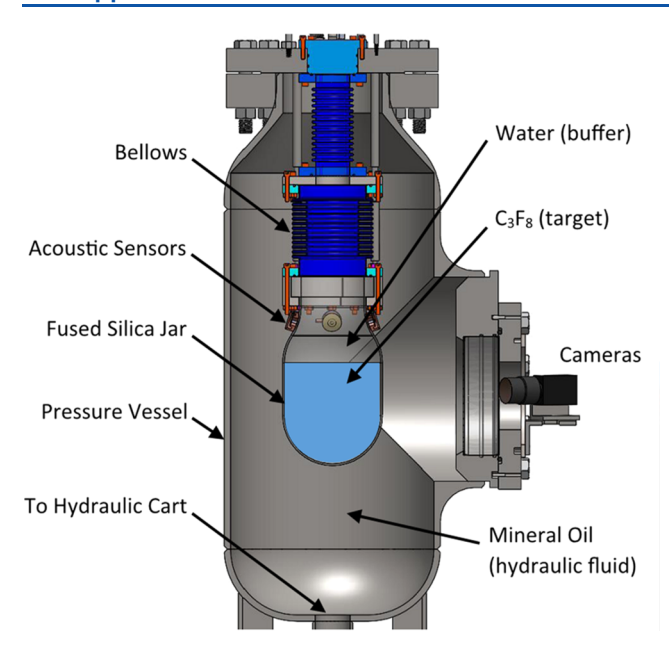
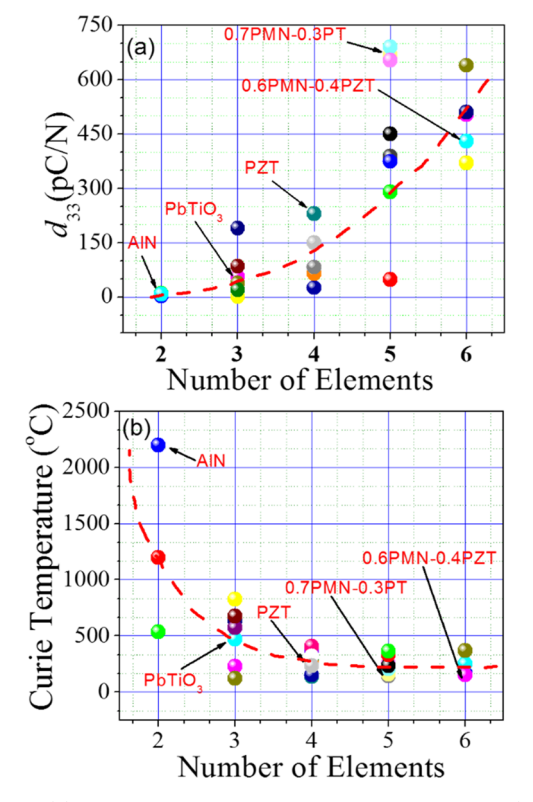


Figure 1. Schematic of the PICO-2L bubble chamber.



**Figure 2.** (a) Longitudinal piezoelectric charge coefficient  $(d_{33})$  vs number of elements in various piezoelectric materials. (b) Curie temperature vs number of elements in various piezoelectric materials. Only representative piezoelectric materials are marked on the plot. The red dashed line is a guide to the eye.

piezoelectric elements, the piezoelectric response, and the Curie temperature. For example, aluminum nitride (AlN) has a low piezoelectric coefficient but a quite high Curie temperature, as shown in Figure 2. Piezoelectric ceramics based on PbTiO<sub>3</sub> (ternary compound) exhibit a higher piezoelectric coefficient and have a high Curie temperature ( $T_c$ ) of ~490 °C. <sup>13</sup> This makes PbTiO<sub>3</sub>-based piezoelectric materials

attractive for high-temperature applications. <sup>14</sup> Ternary Pb- $(Zr,Ti)O_3$  ceramics exhibit much higher piezoelectric properties around the morphotropic phase boundary (MPB) corresponding to a Zr/Ti ratio of 52/48 with a high  $T_c$  of 390 °C. Thus, piezoelectric ceramics comprised of an optimum number of elements with high piezoelectric coefficients and temperature stability need to be developed.

Here, we demonstrate the synthesis of radiopure piezoelectric ceramics with varying compositions and identify the fundamental figure of merit (FOM) governing the performance of piezoelectric transducers for dark matter detection in the bubble chamber. To obtain radiopure piezoelectric elements, the screened precursors that contain low alphaemitters are used as the starting precursors. Additionally, we performed a screening for <sup>210</sup>Pb, which exists in most of the commercial piezoelectric materials. Utilizing the screened precursors, various piezoelectric ceramics that have different piezoelectric coefficients have been successfully synthesized, incorporating doping and texturing techniques. To investigate the relationship between the piezoelectric coefficients of the radiopure piezoelectric ceramics and acoustic sensing performance, a systematic analysis is conducted between the sensitivity and electromechanical coefficients. The acoustic sensitivity of the transducers fabricated by exploiting the tailored piezoelectric ceramics is evaluated by the air spray method. Through this approach, the figure of merit (FOM) of the piezoelectric acoustic sensing performance is determined. Using this FOM, a high-acoustic sensitivity radiopure piezoelectric material is demonstrated.

### ■ RESULTS AND DISCUSSION

Screening of Precursors for Radiopure Piezoelectric Ceramics. The screening of the precursor powders was first carried out to minimize the content of the alpha-emitters <sup>238</sup>U and <sup>232</sup>Th, which generate a significant neutron background in dark matter detection. Screened precursor powders were used as starting raw materials to synthesize various PbZr<sub>0.52</sub>Ti<sub>0.48</sub>O<sub>3</sub> (PZT)-based piezoelectric ceramics. The piezoelectric ceramics prepared from the screened precursors were low in alpha-emitters (9.77  $\pm$  1.68 ppb  $^{238}$ U and 20.95  $\pm$  4.78 ppb <sup>232</sup>Th); see Figure 3a compared to commercial piezoelectric ceramics. The achieved reductions in <sup>238</sup>U and the <sup>232</sup>Th chain factors were ~400 and ~60, respectively. However, the screened piezoelectric elements still exhibited a <sup>210</sup>Pb content, which is similar to that in commercial piezoelectric ceramics, as shown in Figure 3b. The <sup>210</sup>Pb contents were derived from the 46 keV gamma emission detected with a dedicated p-type lowbackground "well" HPGe detector at the underground 6 m.w.e. LASR laboratory of the University of Chicago. This detector type and geometry are necessary to identify low-energy emissions with significant efficiency. The simulations of the detection efficiency used to obtain the 210Pb concentration were sanctioned via calibrations using a liquid <sup>210</sup>Pb source of known strength. A <sup>210</sup>Pb concentration of ~260 Bq/kgPZT was measured for the screened piezoelectric element. 210 Pb is typically found in out-of-equilibrium enhanced concentrations in lead-containing materials. This is due to the chemical affinity of the naturally occurring (<sup>238</sup>U chain) <sup>210</sup>Pb in any materials (e.g., coke, limestone, etc.) coming in contact with the lead ore during its sintering. This leads to its absorption and preferential concentration in the molten lead. Therefore, most of the commercial lead-based piezoelectric materials have <sup>210</sup>Pb, which creates additional issues through increased

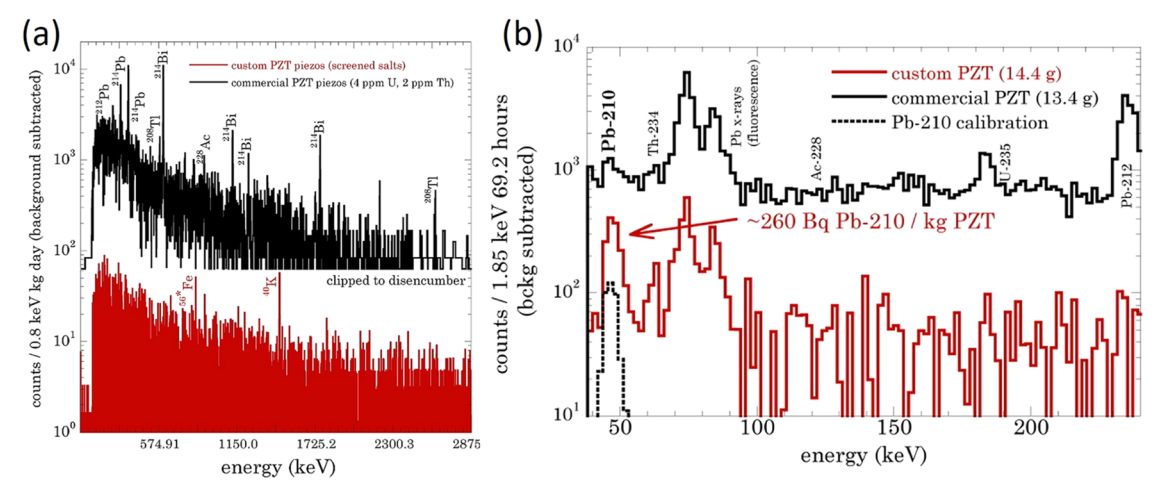
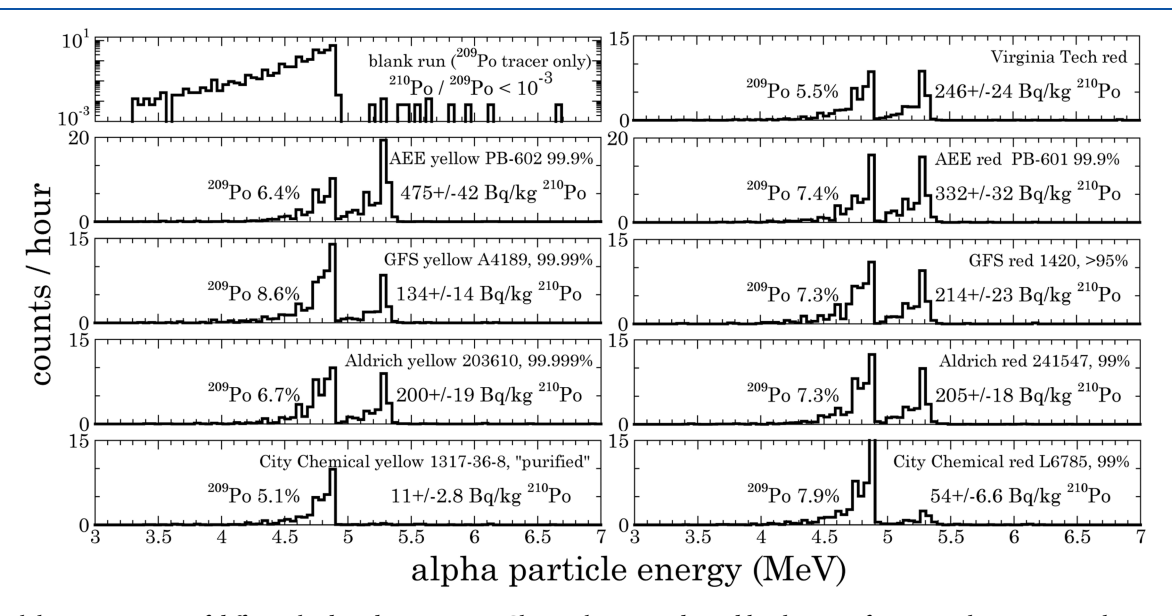


Figure 3. (a) Comparison between the  $^{238}$ U and  $^{232}$ Th activity of commercial piezoelectric materials (Ferroperm PZT) and radiopure piezoelectric material manufactured in this work. (b)  $^{210}$ Pb content of commercial and radiopure piezoelectric materials (0.55  $\pm$  0.12 counts/s expected from simulation, 0.63 count/s observed, calibration not to scale in this figure).



**Figure 4.** Alpha-spectroscopy of different lead oxide precursors. Chemical purity indicated by the manufacturer is shown next to the sample name: as expected, no correlation is found between this chemical purity and <sup>210</sup>Pb content, in view of its origin.

background radiation. In the case of lead-based piezoelectric ceramics, this contamination is introduced via PbO or Pb<sub>3</sub>O<sub>4</sub> precursors. These piezoelectric materials, already dominated by the  $(\alpha, n)$  contribution from their <sup>210</sup>Pb content, were expected to result in 0.46 counts/year from <sup>210</sup>Pb as compared to 1.1 ×  $10^{-2}$  counts/year from the remaining <sup>238</sup>U and <sup>232</sup>Th chains. Such piezoelectric materials are expected to introduce an inadmissible source of weakly interacting massive particle (WIMP)-like recoils in the larger COUPP 60 kg chamber. However, to get more radiopure piezoelectric ceramics, lead-free perovskites can be developed with superior properties, which have lower mass density and lesser background radiation compared to lead-based ceramics (Figure S7).

To develop new radiopure piezoelectric materials with a reduced concentration of <sup>210</sup>Pb, a technique to scan lead oxides with a lower <sup>210</sup>Pb content was developed. Figure 4 shows the alpha-spectroscopy of different lead oxide samples. The peak on the left is from a <sup>209</sup>Po tracer used to determine the efficiency of radiochemical extraction of polonium from the salt and alpha-detection efficiency. The total efficiency is

shown as a percentage of the <sup>209</sup>Po aliquot activity added. The lead oxide used in the developed radiopure Pb-based piezoelectric material (top right) is a factor of  $\sim$ 25 higher in  $^{210}$ Po content than the newly identified yellow oxide (bottom left) to be used in 60 kg-chamber third-generation radiopure piezoelectric materials and beyond. The degraded energy resolution of the alpha-peaks is intentional, by using a suboptimal vacuum in the alpha-counter as a safeguard against recoil-induced contamination of the low-background silicon detector. Figure 5 shows a comparison of the measured content of 210Pb in different lead oxide samples, using an HPGe "well" detector (46 keV gamma emission) and a radiochemical technique, leading to the deposition of its <sup>210</sup>Po daughter on copper planchettes, followed by low-background alpha-counting using a silicon detector. This technique was found to be much more reliable and faster than the first method (hours vs weeks), especially for the low levels of <sup>210</sup>Pb to be used in piezoelectric materials. This scanning resulted in the identification of lead oxide with an extremely lower concentration (by a factor of 25) of <sup>210</sup>Pb. Utilizing this lead

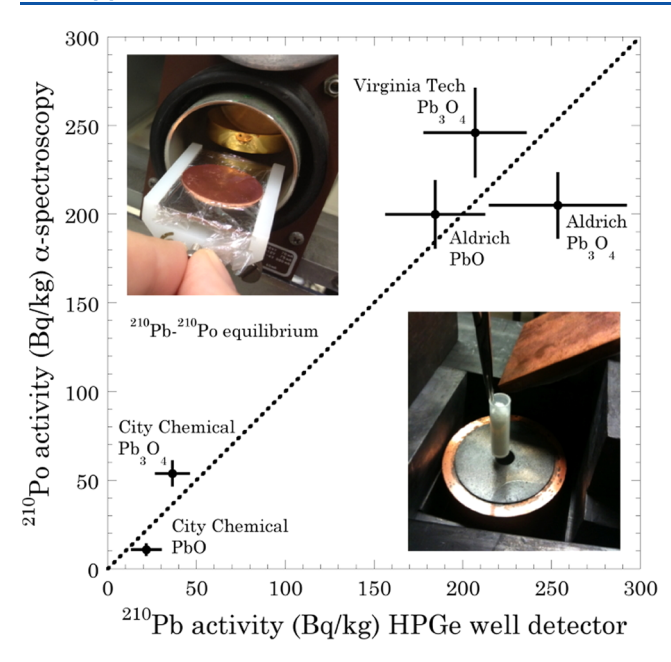


**Figure 5.** Comparison of the measured content of <sup>210</sup>Pb in different lead oxide powders.

oxide precursor, various piezoelectric ceramics were synthesized without any concern about the  $(\alpha, n)$  neutron background.

Synthesis and Electromechanical Characteristics of **Piezoelectric Ceramics.** Based on the screened precursors, binary PbTiO<sub>3</sub> (PTO), ternary PbZr<sub>0.52</sub>Ti<sub>0.48</sub>O<sub>3</sub> (PZT), and quaternary 0.675Pb(Mg<sub>1/3</sub>Nb<sub>2/3</sub>)O<sub>3</sub>-0.325PbTiO<sub>3</sub> (PMN-PT) compounds were synthesized. Figure 6a shows the shapes and sizes of the piezoelectric ceramics used for fabricating transducers. PZT ceramics around the morphotropic phase boundary (MPB) composition exhibit outstanding piezoelectric properties due to increased contributions from ferroelectric domain states assisting in polarization enhancement. However, pristine PZT materials usually contain large amounts of intrinsic defects (due to Pb volatility), resulting in high leakage current, poor fatigue properties, and low piezoelectric coefficients. To obtain stable and outstanding piezoelectric properties in the PZT ceramics, Nb substitution was introduced into the PZT lattice. We found that 5% Nb doping in PZT optimally reduces the intrinsic oxygen vacancies and facilitates polarization rotation due to increased domain wall mobility. This results in an improved fatigue resistance and enhanced piezoelectric coefficients for the PZT ceramics (Table 1). Nb-doped PZT ceramics exhibit a higher piezoelectric charge constant ( $d_{33}$ ) of ~ 380 pC/N compared to that of the pristine PZT ( $d_{33} \sim 210 \text{ pC/N}$ ). Details on the comparative piezoelectric and structural properties between pristine PZT and Nb-doped PZT are provided in the Supporting information, Section S1. Nb-doped PZT was utilized for the radiopure piezoelectric transducer fabricated in this study.

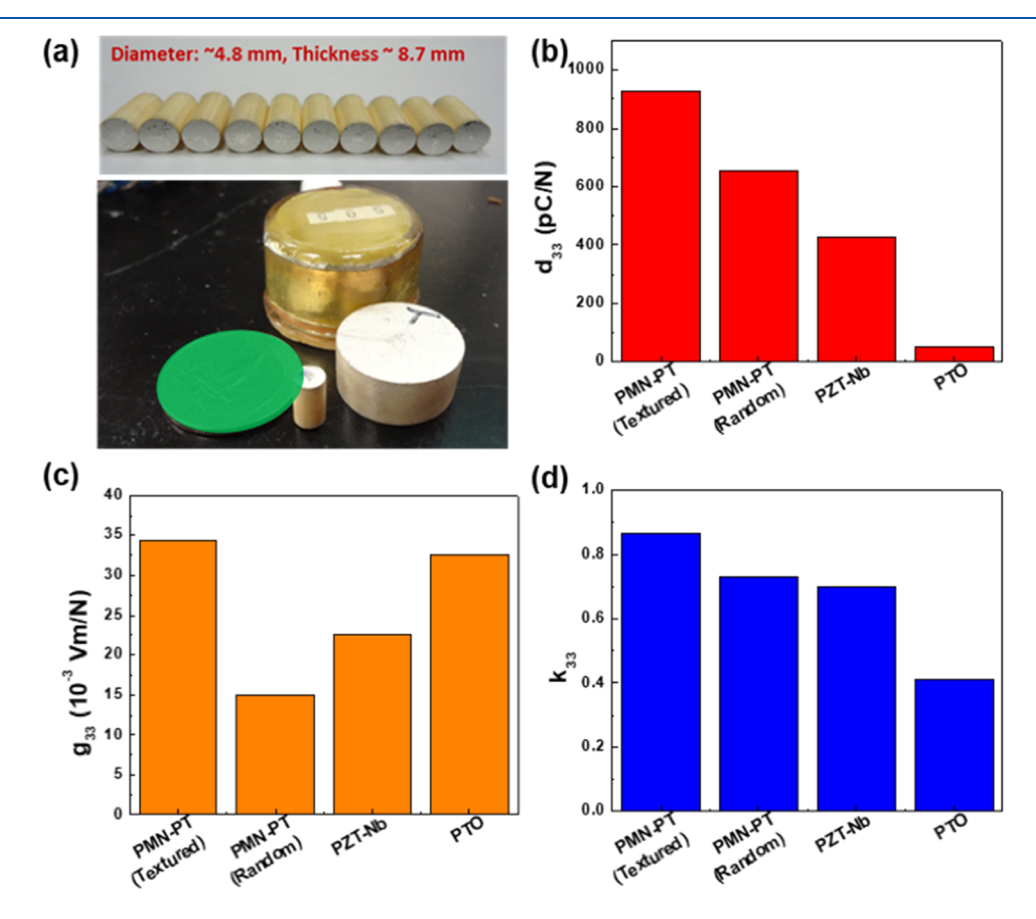


**Figure 6.** (a) Radiopure piezoelectric elements having different sizes and transducers synthesized using the piezoelectric elements. (b) Piezoelectric coefficient  $d_{33}$  of piezoelectric ceramics (c) Piezoelectric coefficient  $g_{33}$  of piezoelectric ceramics. (d) Electromechanical coupling factor  $k_{33}$  of piezoelectric ceramics.

Table 1. Piezoelectric Properties of Piezoelectric Ceramics

	PMN-PT (random)	PMN-PT (textured)	Nb-doped PZT	РТО
$arepsilon_{ m r}$	4959	3048	2151	173
$s_{33}^{D}$ (×10 <sup>-12</sup> m <sup>2</sup> /N)	8.7	10.48	9.79	8.0
$k_{33}$	0.73	0.867	0.70	0.41
$k_{33}$ $s_{33}^{E}$ $(\times 10^{-12} \text{ m}^2/\text{N})$ $d_{33} \text{ (pC/N)}$	18.5	42.3	19.4	9.6
$d_{33}$ (pC/N)	656	926	428	50
$g_{33} \times 10^{-3} \text{ Vm/N}$	14.9	34.3	22.5	32.5

In addition to the Nb-doped PZT, PMN-PT ceramics with a random orientation were synthesized through a solid-state reaction to explore them as a possible future composition to further improve on radiopurity. PMN-PT is a soft piezoelectric material that has high piezoelectric coefficients and high dielectric permittivity. Therefore, the  $d_{33}$  value of the polycrystalline PMN-PT (656 pC/N) is much higher than that of Nb-doped PZT as shown in Table 1, but the piezoelectric voltage coefficient  $(g_{33})$ , which is related to the electric potential generated by the external strain, is much lower than that of other piezoelectric materials because of the extremely high dielectric permittivity ( $\sim$ 5000). A high  $g_{33}$  is an important factor to achieve high acoustic sensitivity, as the output signal from the piezoelectric transducers is correlated to the stress-induced piezoelectric potential. To tailor the piezoelectric coefficients of the PMN-PT, we utilized texturing of the PMN-PT ceramics, which results in high

 $d_{33}$  (~1000 pC/N) as well as high  $g_{33}$ , as compared to Nbdoped PZT and random PMN-PT. The PMN-PT textured ceramics were prepared using the templated grain growth (TGG) method. Texture formation is based on the nucleation and growth of the PMN-PT matrix on aligned BaTiO3 template crystals. The micrographs of textured and randomly oriented ceramics are provided in the Supporting information (Figure S7). The synthesis procedure for textured piezoelectric ceramics and their detailed structural characterization can be found in detail elsewhere.  $^{15,16}$  The increase of  $d_{33}$  was attributed to the engineered domain state in the <001> textured ceramics in a similar fashion as that of <001> oriented single crystals. In a rhombohedral single crystal, the domain configurations with the equivalent <111> polarization exhibit a high piezoelectric response along the <001> direction. The enhanced g<sub>33</sub> was related to the reduced dielectric constant of textured materials due to the presence of templates with a low dielectric permittivity. This phenomenon is analogous to the high  $g_{33}$  obtained in the piezoelectric single crystal-polymer composite.

To investigate the influence of the piezoelectric coefficients on the acoustic sensitivity of the transducers, polycrystalline PTO ceramics with the same dimensions were prepared through the conventional solid-state reaction method. As the PTO ceramic has higher  $g_{33}$  but lower  $d_{33}$  and  $k_{33}$  compared to the Nb-doped PZT and random PMN-PT ceramics, this approach allows delineating parameters that is the most important factor toward the sensitivity of the acoustic transducers. All of the piezoelectric properties of the ceramics

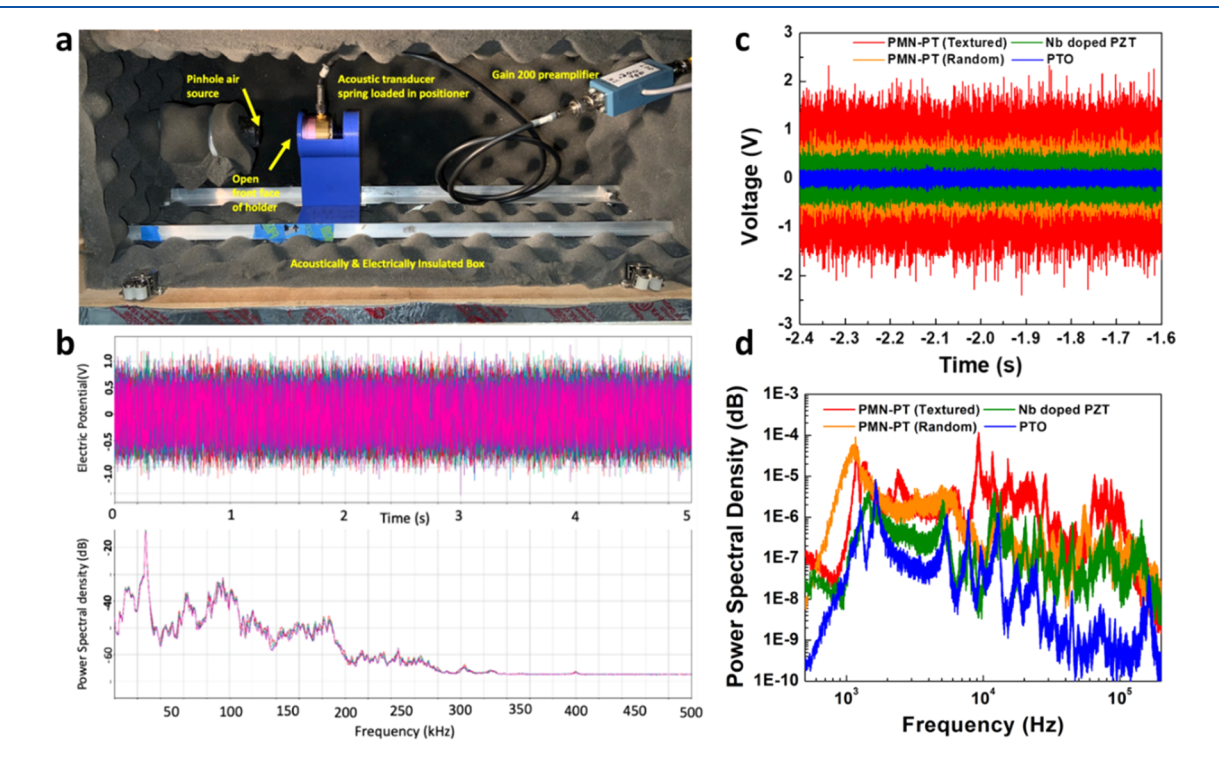


Figure 7. (a) Air spray test apparatus. The source is a pinhole jet with pressure-regulated machine air controlled at 3 psi(g). The 3D-printed transducer holder (blue) allows reproducible experimental conditions for all transducers tested. The front face of the holder is open to the spray source. Acoustic sensitivity of the piezoelectric transducers. (b) Verification of constancy: A single transducer was inserted into the apparatus, air pressure was set, and the response of the acoustic transducer was recorded. This was repeated five times, with the transducer removed, pressure reset, and the transducer reinserted each time. Electric potential and power spectral density for all five runs are shown below to verify the repeatability of the measurement. (c) Voltage output amplitude from the piezoelectric transducers. (d) Power spectral density as a function of the output frequency.

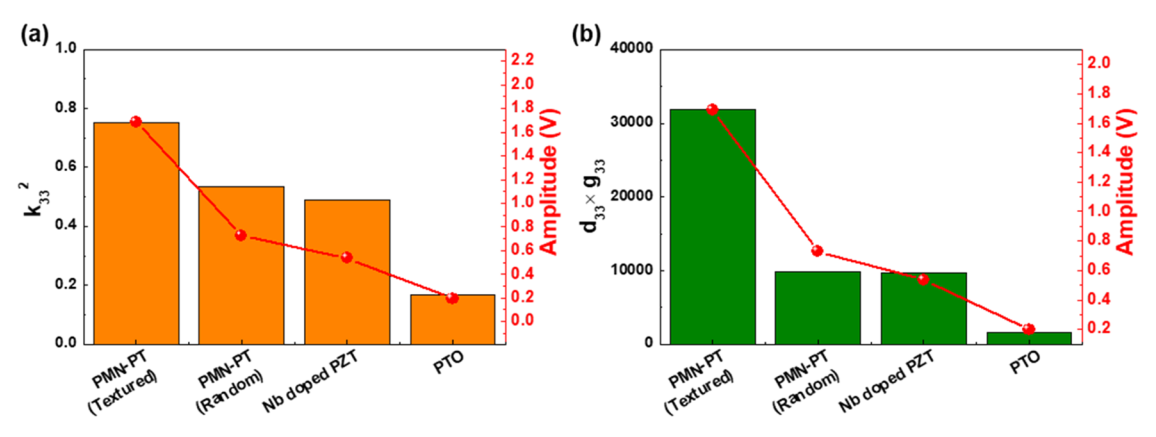


Figure 8. (a) Relationship between  $k_{33}^2$  and acoustic amplitude. (b) Relationship between  $d_{33} \times g_{33}$  and acoustic amplitude.

are provided in Table 1. Figure 6b,c shows the  $d_{33}$  and  $g_{33}$ values of the synthesized piezoelectric ceramics, respectively. These two coefficients represent the electrical output of the piezoelectric ceramics in response to the external mechanical input. The parameter  $d_{33}$  can be defined as the amount of the electric charge (C) generated along the longitudinal direction when the force (N) is applied onto the piezoelectric ceramic in the same direction, and  $g_{33}$  indicates the electric field (V/m)generated across the longitudinal direction when the pressure (N/m<sup>2</sup>) is applied onto the piezoelectric ceramic along the same direction. The magnitude of  $d_{33}$  increases with increasing number of chemical elements, while  $g_{33}$  tends to decrease with increasing number of chemical elements. Interestingly, the PMN-PT textured ceramic exhibits the highest  $d_{33}$  and  $g_{33}$ values among all the samples considered in this study. Moreover, the electromechanical coupling factor, which represents the transduction efficiency of the piezoelectric materials, is also high in the textured PMN-PT ceramics. Therefore, we can expect that the PMN-PT textured ceramic has superior acoustic sensitivity compared to the other samples.

Acoustic Sensitivity of Piezoelectric Transducers under Random Input Frequency. To define an effective FOM for the acoustic sensing performance in the broad frequency range relevant to bubble chamber events, the acoustic sensitivity of the developed piezoelectric transducers was compared by using an air spray apparatus, shown in Figure 7a. The air spray source is a pressure-regulated (3 psi) pinhole leak drilled into a plumbing block. The spray source is inside an acoustically isolated box, which is also a Faraday shield grounded to the oscilloscope (Tektronix DPO 5104 1 GHz) used to record the transducer response. Transducers were mounted in 3D-printed holders inside the box, allowing them to have a reproducible position with respect to the air source. To verify that spray test variations were not due to the variability of the air source or the positioning of the transducers in the apparatus, a single transducer (a standard Nb-doped PZT transducer that was not part of the composition test batch) was inserted, and the air pressure regulator was reset five times to 3 psi(g) for 5 s-long sprays. The electrical response was recorded for five independent sprays, and a power spectral density was calculated from using the Matlab PWELCH function. The five runs exhibit nearly identical responses to the air source (Figure 7b), verifying that tests of various transducers are conducted under the same conditions.

Four types of transducers were tested in this apparatus with 1 s-long sprays at 2 Ms/s and a record length of 2M, and the PSD was again calculated with Matlab, window = hanning (250 000), noverlap = 50%, and DFT = 2 097 152. The pressure of the air spray source was set to 6 psi(g) for this test. The results of test are shown in Figure 7c. For nearly the entire band relevant for the PICO dark matter bubble chamber from 1 to 200 kHz, the textured PMN-PT-based transducer was significantly more sensitive than that of the other types, while the random PMN-PT was superior below 1 kHz. We also note that the  $g_{33}$  value of the PMN-PT textured ceramic is quite similar to that of the PTO, but the output amplitude of the PTO is much lower than that of the textured PMN-PT ceramic.

The general FOM for the energy transduction in the piezoelectric materials can be defined in terms of the electromechanical coupling factor (k) as  $^{17}$ 

$$k^2 = \frac{\text{stored electrical energy}}{\text{input mechanical energy}} \tag{1}$$

This FOM represents the transduction rate at the resonance frequency of the piezoelectric materials as the piezoelectric materials maximize the energy storing rate and transduction of the energy between the mechanical input and electrical output at the resonance. In the air spray condition, however, the input source includes various random frequencies ranging from 10 to 300 kHz, as shown in Figure 7c. Note that the developed piezoelectric transducers were found to have a resonance frequency of about 150 kHz. Furthermore, it can be confirmed that the dependence of the longitudinal electromechanical coupling factor  $k_{33}^2$  and transducer output as a function of the various compositions is quite different (Figure 8a). Therefore, it requires us to consider an alternative reliable FOM factor that can cover a broad range of frequencies.

Priya et al. have proposed a dimensionless FOM for the piezoelectric materials in the piezoelectric energy-harvesting transducer as  $^{18}$ 

$$FOM = \left(\frac{k_{ij}^2 \cdot Q_m}{s_{ij}^E}\right)_{\text{on-resonance}} \left(\frac{d_{ij} \cdot g_{ij}}{\tan \delta}\right)_{\text{off-resonance}}$$
(2)

where  $k_{ij}$  is the electromechanical coupling factor,  $Q_{\rm m}$  is the mechanical quality factor,  $s_{ij}^{\rm E}$  is the elastic compliance at the constant electric field,  $d_{ij}$  is the piezoelectric charge coefficient,  $g_{ij}$  is the piezoelectric voltage coefficient, and  $\tan \delta$  is the dielectric loss. From this relation, the output performance of

the piezoelectric materials in off-resonance mode is proportional to  $d_{ii} \times g_{ii}$  (in the case of the longitudinal mode, this is  $d_{33} \times g_{33}$ ), while  $k_{ii}^2$  and  $Q_{m}$  should be considered to determine the output performance at the resonance frequency. Since our frequency range is wide, covering both resonance and offresonance frequencies, it is expected that the off-resonance parameter will be more relevant here. Interestingly, the output amplitude value generated from the piezoelectric transducers shows an increasing trend with the  $d_{33} \times g_{33}$  product, as shown in Figure 8b. This indicates that  $d_{33} \times g_{33}$  of the piezoelectric elements, called the off-resonance transduction coefficient, is more dominant in determining the acoustic sensitivity of the transducer in response to the random frequency inputs. This finding provides the design criterion for the piezoelectric elements in the acoustic transducers to enhance the acoustic sensitivity. We believe that by building upon this study, the development of the radiopure piezoelectric acoustic transducers can be accelerated to improve the sensing ability in bubble chambers. This design criterion can be utilized to design and develop an emerging class of lead-free piezoelectric materials, which will further have advantages in reducing the background noise. A brief description of the potential lead-free materials is provided in the Supporting information.

#### CONCLUSIONS

In summary, we have developed a screening method to identify highly radiopure precursors with low <sup>238</sup>U, <sup>232</sup>Th, and <sup>210</sup>Pb contents to minimize the  $(\alpha, n)$  neutron background. Using the radiopure precursors, various piezoelectric ceramics that possess different piezoelectric coefficient values were synthesized to investigate the relationship between piezoelectric coefficients and acoustic sensitivity in the random frequency range from 1 to 200 kHz. The piezoelectric coefficients of the ceramics were tailored by using texturing and doping. The acoustic sensitivity of the fabricated piezoelectric transducers was systematically measured to determine the role of electromechanical coefficients. From the results, we found that the  $d_{33} \times g_{33}$  value of the piezoelectric ceramic mainly determines the acoustic sensitivity of the transducer under a wide input frequency range. Among the various piezoelectric ceramics, textured PMN-PT ceramics exhibit superior acoustic sensitivity in the overall frequency range because of the high  $d_{33} \times g_{33}$  value.

### METHODS

Piezoelectric random ceramics, including undoped Pb(Zr,Ti<sub>0.48</sub>)O<sub>3</sub> (PZT), 5 mol % Nb-doped PZT, 0.675Pb(Mg<sub>1/3</sub>Nb<sub>2/3</sub>)O<sub>3</sub>-0.325PbTiO<sub>3</sub> (PMN-PT), and (Pb<sub>0.8725</sub>Sm<sub>0.085</sub>)(Ti<sub>0.98</sub>Mn<sub>0.02</sub>)O<sub>3</sub> (PTO), were synthesized using a conventional solid-state reaction method. In order to synthesize the radiopure piezoelectric ceramics, all raw oxide precursor powders were screened using a lowbackground HPGe detector at the 6 m.w.e. LASR underground laboratory of the University of Chicago. The stoichiometric amounts of radiopure precursors, PbO (Yellow, Purified, City Chemicals LLC), ZrO<sub>2</sub> (Puratronic, 99.978%, Alfa Aesar), TiO<sub>2</sub> (Pursis, Sigma-Aldrich), Nb<sub>2</sub>O<sub>5</sub> (99.99%, Sigma-Aldrich), and MgNb<sub>2</sub>O<sub>6</sub> (99.9%, Alfa Aesar), used for synthesis were ball-milled with ethanol (Anhydrous, 99.5%, Sigma-Aldrich) as a solvent for 24 h. The resulting slurry was dried at 80 °C for 6 h followed by calcination at 800 °C for 2 h. The calcined powder was again ball-milled for 48 h followed by drying and sieving. These powders were pressed into a cylindrical mold. The cold isostatic press (CIP) was used to increase the density of the green body. The specimens were sintered at high temperatures from 1200 to 1300 °C for 4 h for achieving high-density ceramics. The <001>

textured 0.675Pb $(Mg_{1/3}Nb_{2/3})O_3$ -0.325PbTi $O_3$  (PMN-PT textured) piezoelectric ceramics were synthesized by the templated grain growth method. Precursors with a composition corresponding to 0.675Pb- $(Mg_{1/3}Nb_{2/3})O_3$ -0.325PbTiO<sub>3</sub> (PMN-PT) were used as matrix powders. The precursor powders were synthesized by a conventional solid-state reaction. BaTiO3 (BT) platelets were used as the template for texturing PMN-PT. The templates were synthesized by the topochemical microcrystal conversion (TMC) method. The BT templates were aligned in the PMN-PT matrix powders by the tapecasting processing method. 15,16 For tape casting, a slurry was prepared by mixing the PMN-PT matrix powders with BT template platelets, an organic binder, and solvents and then subjected to tape casting by using a doctor blade with a height of 200  $\mu$ m. The dried tapes were cut, stacked, and laminated at 70 °C under 20 MPa for 15 min. The green samples were heated to 600 °C for 1 h with a heating rate of 0.3 C/min for binder burnout and then sintered at 1150 °C for 10 h.

To measure the electrical properties, silver electrodes were applied on both flat surfaces of the piezoelectric ceramics, and the electrical poling was performed at 145 °C for 15 min. The longitudinal piezoelectric constant ( $d_{33}$ ) was measured by the Berlincourt method. The impedance vs frequency measurements was performed using an HP4194A impedance analyzer. Room-temperature XRD spectra were recorded for each sample by using a Philips X'pert Pro X-ray diffractometer (Almelo, the Netherlands). The surface morphology of the sintered samples was observed using a LEO Zeiss 1550 (Zeiss, Munich, Germany) scanning electron microscope (SEM). To observe the ferroelectric domain structure, the samples were polished to a thickness under 30  $\mu$ m, and piezoelectric force microscopy (PFM, Bruker) was performed on the surface of the samples.

#### ASSOCIATED CONTENT

# Supporting Information

The Supporting Information is available free of charge at https://pubs.acs.org/doi/10.1021/acsaelm.3c01116.

SEM micrographs, XRD, and electrical properties of piezoelectric ceramics (PDF)

# AUTHOR INFORMATION

# **Corresponding Author**

Deepam Maurya — Bio-inspired Materials and Devices Laboratory (BMDL), Center for Energy Harvesting Materials and Systems (CEHMS), Virginia Tech, Blacksburg, Virginia 24061, United States; ⊚ orcid.org/0000-0003-3409-0975; Email: mauryad@vt.edu

# Authors

Min Gyu Kang – Department of Materials Science and Engineering, Penn State University, University Park, Pennsylvania 16801, United States

Yongke Yan – Department of Materials Science and Engineering, Penn State University, University Park, Pennsylvania 16801, United States

Hyun-Cheol Song — Electronic Materials Research Center, Korea Institute of Science and Technology, Seoul 136-791, South Korea; KIST-SKKU Carbon-Neutral Research Center, Sungkyunkwan University (SKKU), Suwon 16419, Republic of Korea; orcid.org/0000-0001-5563-9088

Lijuan Yang — Bio-inspired Materials and Devices Laboratory (BMDL), Center for Energy Harvesting Materials and Systems (CEHMS), Virginia Tech, Blacksburg, Virginia 24061, United States

Ilan Levine – Department of Physics and Astronomy, Indiana University South Bend, South Bend, Indiana 46634, United States

- Edward Behnke Department of Physics and Astronomy, Indiana University South Bend, South Bend, Indiana 46634, United States
- Haley Borsodi Department of Physics and Astronomy, Indiana University South Bend, South Bend, Indiana 46634, United States
- Drew Fustin KICP and Department of Physics, Enrico Fermi Institute, University of Chicago, Chicago, Illinois 60637, United States
- Aman Nanda Department of Materials Science and Engineering, Penn State University, University Park, Pennsylvania 16801, United States
- Juan I. Collar KICP and Department of Physics, Enrico Fermi Institute, University of Chicago, Chicago, Illinois 60637, United States; Donostia International Physics Center (DIPC), 20018 Donostia-San Sebastian, Spain
- Shashank Priya Department of Materials Science and Engineering, Penn State University, University Park, Pennsylvania 16801, United States

Complete contact information is available at: https://pubs.acs.org/10.1021/acsaelm.3c01116

#### **Notes**

The authors declare no competing financial interest.

## ACKNOWLEDGMENTS

Y.Y., S.P., A.N., and I.L. acknowledge the financial support through the National Science Foundation award number DMR-1936432. Other coauthors providing supporting data for this study gratefully acknowledge the financial support from the National Science Foundation through grant number PHY-1242637.

#### REFERENCES

- (1) Aubin, F.; Auger, M.; Genest, M. H.; Giroux, G.; Gornea, R.; Faust, R.; Leroy, C.; Lessard, L.; Martin, J. P.; Morlat, T.; Piro, M. C.; Starinski, N.; Zacek, V.; Beltran, B.; Krauss, C. B.; Behnke, E.; Levine, I.; Shepherd, T.; Nadeau, P.; Wichoski, U.; Pospisil, S.; Stekl, I.; Sodomka, J.; Clark, K.; Dai, X.; Davour, A.; Levy, C.; Noble, A. J.; Storey, C. Discrimination of Nuclear Recoils from Alpha Particles with Superheated Liquids. New J. Phys. 2008, 10 (10), No. 103017.
- (2) Panda, P. K.; Sahoo, B. PZT to Lead Free Piezo Ceramics: A Review. Ferroelectrics 2015, 474 (1), 128–143.
- (3) Behnke, E.; Behnke, J.; Brice, S. J.; Broemmelsiek, D.; Collar, J. I.; Conner, A.; Cooper, P. S.; Crisler, M.; Dahl, C. E.; Fustin, D.; Grace, E.; Hall, J.; Hu, M.; Levine, I.; Lippincott, W. H.; Moan, T.; Nania, T.; Ramberg, E.; Robinson, A. E.; Sonnenschein, A.; Szydagis, M.; Vázquez-Jáuregui, E. First Dark Matter Search Results from a 4-kg CF 3I Bubble Chamber Operated in a Deep Underground Site. *Phys. Rev. D* **2012**, *86* (5), No. 052001, DOI: 10.1103/Phys-RevD.86.052001.
- (4) Amole, C.; Ardid, M.; Asner, D. M.; Baxter, D.; Behnke, E.; Bhattacharjee, P.; Borsodi, H.; Bou-Cabo, M.; Brice, S. J.; Broemmelsiek, D.; Clark, K.; Collar, J. I.; Cooper, P. S.; Crisler, M.; Dahl, C. E.; Daley, S.; Das, M.; Debris, F.; Dhungana, N.; Farine, J.; Felis, I.; Filgas, R.; Fines-Neuschild, M.; Girard, F.; Giroux, G.; Hai, M.; Hall, J.; Harris, O.; Jackson, C. M.; Jin, M.; Krauss, C. B.; Lafrenière, M.; Laurin, M.; Lawson, I.; Levine, I.; Lippincott, W. H.; Mann, E.; Martin, J. P.; Maurya, D.; Mitra, P.; Neilson, R.; Noble, A. J.; Plante, A.; Podviianiuk, R. B.; Priya, S.; Robinson, A. E.; Ruschman, M.; Scallon, O.; Seth, S.; Sonnenschein, A.; Starinski, N.; Štekl, I.; Vázquez-Jáuregui, E.; Wells, J.; Wichoski, U.; Zacek, V.; Zhang, J. Dark Matter Search Results from the PICO-2L C3 F8 Bubble Chamber. *Phys. Rev. D* 2016, 93 (5), No. 052014, DOI: 10.1103/PhysRevLett.114.231302.

- (5) Glaser, D. A. Some Effects of Ionizing Radiation on the Formation of Bubbles in Liquids. *Phys. Rev.* **1952**, *87* (4), 665.
- (6) Behnke, E.; Collar, J. I.; Cooper, P. S.; Crum, K.; Crisler, M.; Hu, M.; Levine, I.; Nakazawa, D.; Nguyen, H.; Odom, B.; Ramberg, E.; Rasmussen, J.; Riley, N.; Sonnenschein, A.; Szydagis, M.; Tschirhart, R. Spin-Dependent WIMP Limits from a Bubble Chamber. *Science* **2008**, *319* (5865), 933–936, DOI: 10.1126/science.1149999.
- (7) Seitz, F. On the Theory of the Bubble Chamber. *Phys. Fluids* **1958**, 1 (1), 2-13.
- (8) Fustin, D. A. First Dark Matter Limits from the COUPP 4 kg Bubble Chamber at a Deep Underground Site; The University of Chicago: IL, 2012.
- (9) Jaffe, B.; Cook, W. R., Jr.; Jaffe, H. Piezoelectric Ceramics, 1st ed.; Academic Press: London and New York, 1971.
- (10) De, U.; Sahu, K. R.; De, A. Ferroelectric Materials for High Temperature Piezoelectric Applications. *Solid State Phenom.* **2015**, 232, 235–278, DOI: 10.4028/www.scientific.net/SSP.232.235.
- (11) Zhang, S.; Yu, F. Piezoelectric Materials for High Temperature Sensors. J. Am. Ceram. Soc. 2011, 94 (10), 3153–3170.
- (12) Park, S. E.; Shrout, T. R. Characteristics of Relaxor-Based Piezoelectric Single Crystals for Ultrasonic Transducers. *IEEE Trans. Ultrason. Ferroelectr. Freq. Control* **1997**, 44 (5), 1140–1147.
- (13) Ueda, I.; Ikegami, S. Piezoelectric Properties of Modified PbTiO3 Ceramics. *Ipn. J. Appl. Phys.* **1968**, 7 (3), 236.
- (14) Palkar, V. R.; Purandare, S. C.; Pinto, R. Breakthrough in Densification of Ferroelectric PbTiO3 with Si as Sintering Aid. *Mater. Lett.* **2000**, 43 (5–6), 329–334.
- (15) Yan, Y.; Cho, K. H.; Priya, S. Templated Grain Growth of (001)-Textured 0.675Pb(Mg1/3Nb2/3)O3-0.325PbTiO3 Piezoelectric Ceramics for Magnetic Field Sensors. *J. Am. Ceram. Soc.* **2011**, 94 (6), 1784-1793.
- (16) Yan, Y.; Wang, Y. U.; Priya, S. Electromechanical Behavior of [001]-Textured Pb(Mg 1/3Nb 2/3)O 3-PbTiO 3 Ceramics. *Appl. Phys. Lett.* **2012**, *100* (19), No. 192905.
- (17) Uchino, K. Ferroelectric Devices. Marcel Dekker 2000. https://scholar.google.com/scholar?hl=en&as\_sdt=0%2C39&q=Uchino%2C+K.+%282000%29+Ferroelectric+Devices.+Marcel+Dekker%2C+New+York&btnG (accessed 2023 -05 -01).
- (18) Priya, S. Criterion for Material Selection in Design of Bulk Piezoelectric Energy Harvesters. *IEEE Trans. Ultrason. Ferroelectr. Freq. Control* **2010**, *57* (12), 2610–2612, DOI: 10.1109/TUFFC.2010.1734.